Characterization of powellite-based solid solutions by site-selective time resolved laser fluorescence spectroscopy

Moritz Schmidt,*[a] Stephanie Heck,[a] Dirk Bosbach,[b] Steffen Ganschow,[c] Clemens Walther[d] and Thorsten Stumpf[a]

We present a comprehensive study of the solid solution system $Ca_2(MoO_4)_2$–$NaGd(MoO_4)_2$ on the molecular scale, by means of site-selective time resolved laser fluorescence spectroscopy (TRLFS). Eu^{3+} is used as a trace fluorescent probe, homogeneously substituting for Gd^{3+} in the solid solution crystal structure. Site-selective TRLFS of a series of polycrystalline samples covering the whole composition range of the solid solution series from 10% substitution of Ca^{2+} to the NaGd end-member reveals it to be homogeneous throughout the whole range. The trivalent ions are incorporated into the powellite structure in only one coordination environment, which exhibits a very strong ligand–metal interaction. Polarization-dependent measurements of a single crystal of $NaGd(Eu)(MoO_4)_2$ identify the coordination geometry to be of C_{2v} point symmetry. The S_4 symmetry of the Ca site within the powellite lattice can be transformed into C_{2v} assuming minor motion in the first coordination sphere.

Introduction

Powellite ($CaMoO_4$) is a naturally occurring mineral that forms as an alteration product of molybdenite MoS_2 under oxidizing conditions. Powellite has also been shown to form as a secondary mineral upon corrosion of Mo-bearing high-level nuclear waste (HLW) borosilicate glasses.[1] During this process radionuclides may form thermodynamically stable solid solutions with powellite, and thus remain effectively immobilized after the initial failure of the technological barrier.[1–6] Powellite solid solutions have also recently attracted interest from materials scientists as materials with noteworthy dielectric and optical properties.[7–10]

Powellite crystallizes in the scheelite structure with the space group $I4_1/a$ in which the central Ca^{2+} ion is coordinated by eight singly-bound molybdate groups (Fig. 1). The point symmetry of the Ca site in this structure has been reported as D_{2d}[11] as well as S_4 in synthetic samples.[12] The structure is ideally suited for the formation of solid solutions, as it exhibits significant compositional flexibility.[3] When trivalent ions are

substituted for the divalent Ca^{2+} ion charge compensation has been found to proceed *via* coupled substitution with monovalent cations,[10,13,14] *e.g.* alkali metal ions. This mechanism has been identified for other solid solutions as well.[15] In other
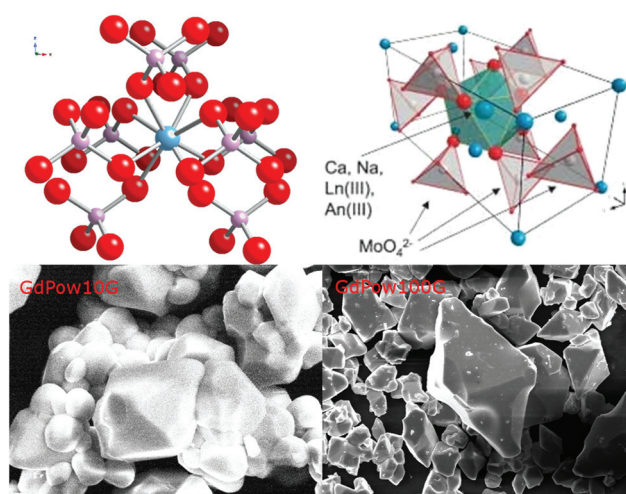

Fig. 1 Top: Coordination of Ca^{2+} in the Ca site of the powellite lattice, blue: Ca, red: O, pink: Mo (left), and unit cell of the powellite structure, blue: Ca, red: O, white: Mo (right). Ca, Na, and Ln are coordinated by eight O belonging to eight unique MoO_4^{2-}-tetrahedra. Bottom: SEM micrographs of the crystal morphology of the series members with 10 and 100% substitution, GdPow10G and GdPow100G, respectively, are shown in the bottom of the figure. The crystallites are approx. 10 μm in size.

[a]*Institute for Nuclear Waste Disposal, Karlsruhe Institute of Technology, Karlsruhe, Germany. E-mail: moritz.schmidt@kit.edu, stephanie.heck@kit.edu, thorsten.stumpf@kit.edu*

[b]*Institut für Energie- und Klimaforschung (IEK-6), Forschungszentrum Jülich, Jülich, Germany. E-mail: d.bosbach@fz-juelich.de*

[c]*Leibniz-Institut für Kristallzüchtung, Berlin, Germany. E-mail: steffen.ganschow@ikz-berlin.de*

[d]*Institut für Radioökologie und Strahlenschutz, Universität Hannover, Hannover, Germany. E-mail: walther@irs.uni-hannover.de*

Ln^{3+}-molybdates defect structures have been identified where two trivalent cations substitute for three divalent calcium ions.[16]

For either application, as a dielectric material or for the immobilization of nuclear waste, the efficacy of the material will depend on its stability. Material stability is again related to material properties such as crystallinity, phase purity, and distribution of the luminescent probe,[9] or radionuclide, respectively. The stability of a solid solution is to a large degree dependent on the stress induced in the lattice by the substitution.[17] Fully understanding the structural effects of a substitution mechanism will require analytical techniques that are capable of probing local structural features in great detail. The overall structure of the solid solution is commonly accessible by X-ray diffraction (XRD) techniques; however, XRD will not easily reveal local structural effects around the guest ion. The local coordination environment of guest ions in a solid solution can be characterized by time-resolved laser fluorescence spectroscopy (TRLFS).[15,18–22] For this study we applied site-selective Eu^{3+} TRLFS at low temperatures ($T < 20$ K), which is particularly efficient for the speciation and characterization of multi-species systems.[18,19,23–26] The technique allows determination of the different species in a system by excitation from the $^7F_0$ ground state to the $^5D_0$ state. In this transition both levels are non-degenerate and thus only one singlet signal is observed for each species. Determination of the number of non-equivalent species is possible by simple counting of observed transitions as long as resolution and line widths allow an unambiguous separation. In addition, the signal position of the F_0 band gives a first indication of the local environment of the respective Eu^{3+} species: stronger coordination generally results in lower energy transition, *i.e.* a stronger bathochromic shift of the signal.[26–28] Consecutive selective excitations of the respective species yield "single species"-emission spectra and -lifetimes. The emission spectra allow identification of the ions coordination environment in this site, using the splitting pattern and the relative intensity of the ($^5D_0 \rightarrow {}^7F_1$)- and ($^5D_0 \rightarrow {}^7F_2$)-transitions, the so-called hypersensitive effect.[29]

We can improve the level of detail of the structural characterization by making use of the polarization dependence of the selection rules for transitions of the Eu^{3+} fluorescence emission.[30] In single crystals, where orientations are not averaged isotropically, emission spectra may show different splitting patterns depending on the polarization direction of the exciting laser and the symmetry of the local coordination environment of Eu^{3+}. For example, if Eu^{3+} were coordinated in the D_{2d} point symmetry suggested for the Ca^{2+} site in the powellite lattice, the ($^7F_0 \rightarrow {}^5D_4$)-excitation and the ($^5D_0 \rightarrow {}^7F_4$)-emission will show a twofold splitting when the laser's polarization plane (with respect to the electric field vector **E**) is perpendicular to the c-axis of the crystal (σ-geometry), but only one when the polarization plane is parallel to this direction (π-geometry).[30] Through procedures described in the literature,[30,31] it is now possible to determine the exact point group of the fluorescent probe's local coordination by measuring significant transitions in the Eu^{3+} spectrum in σ- and π-geometry.

In aqueous systems, the fluorescence of Eu^{3+} can only be effectively quenched by energy transfer to O–H-vibrational modes, due to the magnitude of the energy gap. Under this condition, the number of water molecules coordinating Eu^{3+} can be determined through Horrocks' equation.[32,33] In the presence of transition metals a different path for radiationless deexcitation becomes available, and fluorescence lifetimes are no longer a simple function of the number of water molecules in the first coordination sphere of Eu^{3+}. This effect has been well documented for systems containing Fe, as well as other transition metals[34–36] and can be described theoretically as direct metal-to-metal energy transfer.[37,38] Similar effects were observed for Eu^{3+} fluorescence emission lifetimes in the presence of Mo in this study (see the Results and discussion section).

There are some previous studies on the luminescence of rare earths incorporated into powellite; however, most studies focus on members of the series with low concentrations of the guest ion, and a comprehensive study of a complete solid solution series has to the best of our knowledge not been published thus far. There is also no detailed investigation of the structural effects of the substitution on the powellite lattice. Thomas *et al.* studied solid solutions with the general composition $CaGd_{1-x}NbMoO_8$: xEu^{3+} for x = 5–30%. They find emission spectra with strongly enhanced ($^5D_0 \rightarrow {}^7F_2$)-transitions compared to relatively weak ($^5D_0 \rightarrow {}^7F_1$)-bands upon UV excitation. The ($^5D_0 \rightarrow {}^7F_2$)-transitions are clearly enhanced by the hypersensitive effect, indicating strong coordination. The spectra for series members with 5% to 30% trivalent metal content are very similar; however, a detailed structural analysis was not performed as spectra lack the necessary resolution.[9] Mendoza *et al.* also studied the early members of the solid solution series with up to 7% Ln^{3+} substitution before and after irradiation by Ar and Pb ion beams. Once again the spectra show a strong hypersensitive effect. The spectra show a very complex behavior of the ($^5D_0 \rightarrow {}^7F_0$) band, which was fit using nine Gaussian profiles, pointing to a manifold of different, but similar, coordination environments for the guest ion. The spectra after irradiation are simpler, exhibiting fewer species and a red shift of the ($^5D_0 \rightarrow {}^7F_0$) transition. This suggests a higher degree of order around the trivalent guest ion and a stronger coordination by the $MoO_4{}^-$-ligands.[4]

Here, we present a comprehensive investigation of the solid solution series $Ca_2(MoO_4)_2$–$NaGd(Eu)(MoO_4)_2$ by site-selective time resolved laser fluorescence spectroscopy. Our study comprises the investigation of a full solid solution series from 10% Ca^{2+}-substitution to the Na–Gd-end-member as powder samples, as well as the polarization-dependent characterization of the trivalent ions local environment's structure, and thus the deformation of the lattice around the fluorescent probe.

Experimental

Sample synthesis

Polycrystalline samples. Polycrystalline samples of different compositions were synthesized in a conventional high

temperature procedure from $CaCO_3$, Na_2CO_3, MoO_3, Gd_2O_3, and Eu_2O_3 starting materials. Solid starting materials are mixed in the desired stoichiometry in a mortar and heated to 1000 °C. The solid solution formation is completed after 72 h. A total of six samples were prepared, in which 10%, 30%, 50%, 70%, 90%, and 100% of Ca^{2+} were replaced by Na^+ and Gd^{3+}. Phase purity was checked by SEM and XRD, and stoichiometric composition is assumed for all samples. The samples are labeled according to their degree of substitution as GdPow10G–GdPow100G.

Eu^{3+} is used as the fluorescent probe. To avoid self-quenching effects, Eu^{3+} cannot be used in stoichiometric quantities at the highest concentrations.[3] Gd^{3+} was chosen for "dilution" because of its very similar chemical behavior, and ionic radius (in eight-fold coordination, Eu^{3+}: 1.06 Å, Gd^{3+}: 1.05 Å[39]), and each sample contains an identical concentration of 50 ppm Eu^{3+}. It is to be expected that Gd^{3+} and Eu^{3+} will behave identically in the synthesis procedure.[40]

Single crystal samples. A single crystal was grown from the melt of stoichiometric composition according to the formula $NaGd_{1-x}Eu_x(MoO_4)_2$ with $x = 0.001$ using the Czochralski method. The powder raw material was melted in a 40 ml platinum crucible and left for homogenization for about one hour. A [100] oriented rod prepared from isostructural $NaGd(WO_4)_2$ was used as a seed. The crystal was pulled at 1 mm h^{-1} and rotated at a rate of 10 rpm to improve the temperature homogeneity and melt mixing. All process steps were carried out in air. The grown crystal was 40 mm long, about 20 g in mass, and free of visible defects like cracks or grain boundaries.

Solid phase analysis. The solid powders were analyzed by powder X-ray diffraction (XRD) and scanning electron microscopy (SEM). For XRD approx. 20 mg of dry powder were suspended in ethanol and left to dry on an amorphous silica X-ray sample holder. Measurements were performed on a Bruker D5000 diffractometer using Cu-Kα radiation (1.54 Å) at 40 kV and 40 mA. Diffraction patterns were recorded in the range of 5–80° with 0.01° steps and 1 s collection time. Samples were rotated at an angular speed of 15° s^{-1}. SEM micrographs were recorded with various magnifications using a CamScan FE44 microscope.

Laser fluorescence spectroscopy

To achieve the desired spectral resolution the powder samples were cooled to temperatures below 20 K in a helium refrigerated cryostat. The luminescence was excited by a XeCl excimer pumped dye laser directly exciting Eu^{3+}'s $^5D_0$ level. Coumarin 153 was used as a dye. The luminescence emission signal is recorded time resolved by a fibre coupled optical multichannel system consisting of a polychromator with 300, 600 and 1200 lines per mm gratings and a gated, intensified diode array.

Polarization-dependent measurements were performed using a Fresnel rhomb mounted on a rotating pedestal that allows precise rotation by specified increments. The laser emission is inherently polarized; the polarization plane is, however, unknown. Consequently, the polarization plane was rotated in
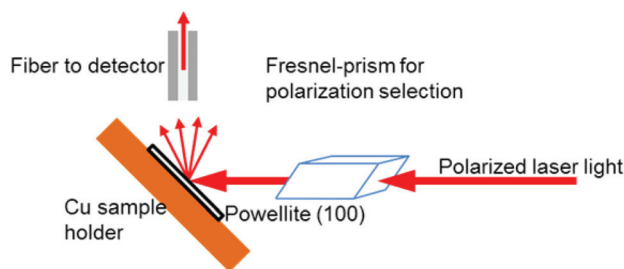

Fig. 2 Schematic representation of the set-up used for the polarization-dependent TRLFS measurements. The angle between sample surface and laser beam and fiber, respectively, is ~45°.

increments of 10° and spectra were taken at each of the orientations to ensure covering the full 90° rotation without missing potential changes in the fluorescence emission. A schematic representation of the setup is shown in Fig. 2. In the experiment a single crystal of $NaGd(Eu)(MoO_4)_2$ was setup in the laser beam so that the polarized laser hits the (100) surface of the crystal in a 45° angle.

All TRLFS data were acquired using the trace amount of Eu^{3+} as a fluorescent probe, and it is presumed that all findings made for Eu^{3+} are equally valid for Gd^{3+} in these samples.

Results and discussion

X-ray powder diffraction

The diffraction patterns of all samples GdPow10G–GdPow100G in the range of 15–80° are presented in Fig. 3 with the diffraction pattern of undoped powellite, grown by the same method described above. The diffraction patterns do not show any significant, or systematic variation with the degree of substitution. All major peaks in the powellite diffraction pattern are clearly resolved and found in the patterns of all samples.
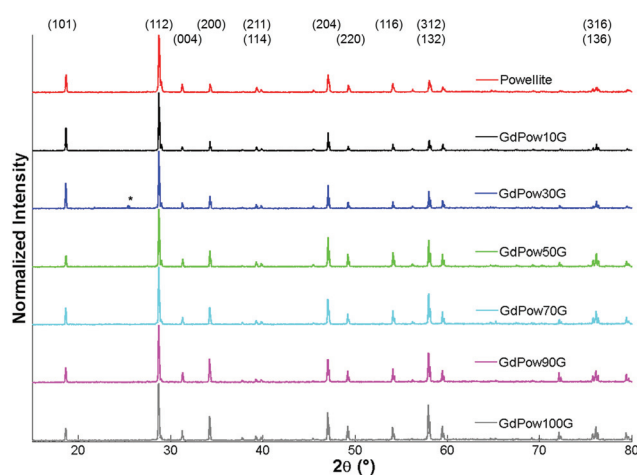

Fig. 3 X-ray diffraction patterns of all samples GdPow10G–100G in the angular range of 15–80°. For comparison, the diffraction from powellite grown by the same method as the doped samples is shown. Major diffraction peaks are labelled with their respective crystallographic index. The symbol * denotes diffraction peaks not found in the powellite diffraction pattern.

There are slight variations in the relative peak intensities; however, these are more likely to be related to specific crystal orientations due to the sample preparation technique than to actual crystallographic differences.

Obviously, even the complete substitution of Ca^{2+} by Na^+ and Gd^{3+} does not affect the bulk crystallography of the solid solution as seen by X-ray powder diffraction. Instead, all samples could be identified as powellite. In order to characterize the structural impact of the substitution it is, thus, essential to use a probe capable of probing structural changes locally.

Moreover, the results indicate a random distribution of Na^+ and Gd^{3+} over the Ca^{2+} lattice sites, as opposed to the formation of a layered structure, contradicting earlier Monte Carlo simulations of the powellite solid solution system, which had predicted an ordering of the cations.[41]

TRLFS of powder sample solid solution series

The excitation spectra of the Eu^{3+} $(^7F_0 \rightarrow {}^5D_0)$-transition of all members of the solid solution series are shown in Fig. 4. All spectra show the same sharp transition that is strongly red-shifted to 580.5 nm. The Na–Gd-end-member is the only exception; here, the signal is slightly less red shifted to 580.3 nm. It is also broader with a full width at half maximum (FWHM) of 0.60 nm compared to 0.27 nm for the other samples. In the spectrum of sample GdPow10G, with the lowest substitution, a second broad asymmetric peak can be recognized at 575.9 nm. A broadening in the signal may be attributed to a distribution of Eu^{3+} over several very similar yet not identical lattice sites. This is corroborated by the fact that the emission spectrum after direct excitation (Fig. 5) shows no such line broadening.

The presence of one dominating signal in all members of the series suggests that there are no or very minor changes in the structure of the local coordination of the trivalent ions
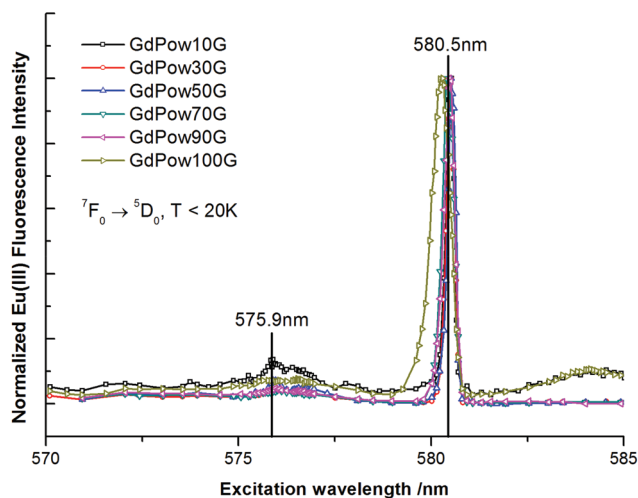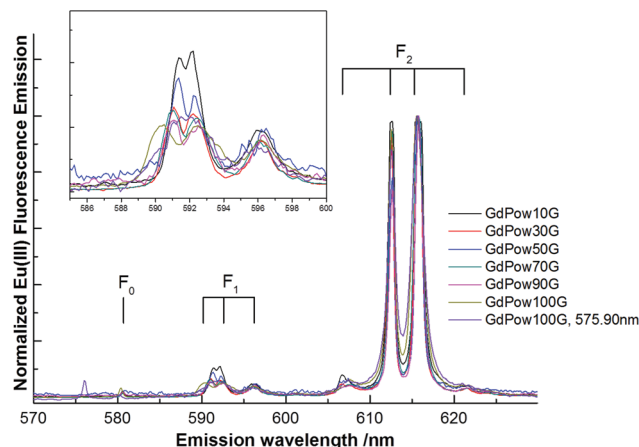

Fig. 5 Emission spectra of all members of the Ca_2MoO_4–$NaGd(Eu)(MoO_4)_2$ solid solution series after direct excitation to $^5D_0$ at $T < 20$ K. For the $NaGdMoO_4$ end-member the emission spectrum after excitation to the hot band at 575.9 nm is shown for comparison.

throughout the whole composition range. The strong red shift of the major species is indicative of incorporation, as had been expected based on the synthesis procedure. The signal's bathochromic shift is stronger than for Eu^{3+} incorporated into other Ca^{2+} mineral phases, e.g. calcite where the six-fold coordination by CO_3^{2-} shifts the $(^7F_0 \rightarrow {}^5D_0)$-transition to 579.6 nm.[15] The eight-fold MoO_4^{2-}-coordination must be inducing a strong splitting of Eu^{3+}'s crystal field levels.[26,42] The emission spectra of the species allow additional insight into the local coordination of the trivalent ions in the solid solution. Emission spectra are shown in Fig. 5.

The emission spectra for all samples of the series show only minor variations. The $(^5D_0 \rightarrow {}^7F_2)$-transition is significantly enhanced in comparison with the $(^5D_0 \rightarrow {}^7F_1)$-transition, due to the hypersensitive effect. The integrated intensity ratio is $(^5D_0 \rightarrow {}^7F_1)/(^5D_0 \rightarrow {}^7F_2) = 1:9$ for GdPow10G, substantiating the assumption of a strong MoO_4^{2-}–Eu^{3+} interaction. The $(^5D_0 \rightarrow {}^7F_2)$-transition exhibits a fourfold splitting, with a threefold splitting in the $(^5D_0 \rightarrow {}^7F_1)$-band. This indicates a tetragonal symmetry. The powder spectra do not allow an unambiguous point symmetry determination, but the observed splitting pattern seems to be in disagreement with both, D_{2d} and S_4 point symmetry, for the Ca^{2+} site in powellite. For a more detailed analysis the polarization-dependence was taken into account (see the next section).

Minor changes can be observed in the specific intensities of single peaks in the $(^5D_0 \rightarrow {}^7F_1)$-band from samples early in the series (10G–50G) and the later members (70G–100G). The splitting pattern does not change, the band shows threefold splitting in all spectra, but the relative intensity of $^7F_1$- and $^7F_2$-band changes slightly. The spectral separation of the single peaks within the band increases with increasing Gd^{3+} substitution. A straightforward interpretation of this effect is not easily possible, but it appears evident that there is a minor change in the local coordination of the Eu^{3+} ion that does not affect the overall symmetry, but rather the efficiency of the

Fig. 4 $(^7F_0 \rightarrow {}^5D_0)$ excitation spectra of Eu^{3+} doped members of the Ca_2MoO_4–$NaGd(Eu)(MoO_4)_2$ solid solution series recorded at low temperatures ($T < 20$ K). The integrated intensity of the $(^5D_0 \rightarrow {}^7F_{1,2})$-transitions (585–630 nm) is plotted as a function of the excitation wavelength.

crystal splitting, *e.g.* by a change in bond distances. The increased splitting suggests a more efficient orbital overlap between the fluorescent probe and the MoO_4^{2-}-ligand, which suggests a shortening of the metal–ligand bond distance. This seems likely as we are replacing a divalent ion by a trivalent ion of nearly identical radius, thus greatly increasing the charge density in the Ca^{2+} lattice site. This assessment is, however, not supported by the lifetime measurements (see below).

Fig. 5 shows the emission of sample GdPow100G after excitation in the minor peak at 575.9 nm (purple line). The emission spectrum is identical to the one observed after selective excitation of the major species, making it appear reasonable that the observed intensity in the excitation spectrum is related to a "hot band" of the major species, rather than to a separate species in the powellite lattice.

For the major species in all the samples fluorescence emission lifetimes were determined. Identical, monoexponential fluorescence decay profiles are measured for all samples, yielding a lifetime of 410 ± 30 μs. No trend with increasing Gd^{3+}-loading is observed, which would have been in support of a continuous decrease in the metal–ligand bond length, as was speculated based on the fluorescence emission spectra. The measured lifetime would correspond to 2.0 H_2O molecules in the first coordination sphere according to Horrocks' equation.[32,33] This is unreasonable considering the synthesis conditions; due to the high temperature synthesis full dehydration can be considered certain for all samples. As described above, the lifetimes are controlled by the non-radiative energy transfer from excited Eu^{3+} to MoO_4^{2-}, and no information on the hydration state of Eu^{3+} can be obtained.

Polarization-dependent TRLFS

The full extent of the lattice distortion induced by the substitution $Na^+ + Gd^{3+} \leftrightarrow 2Ca^{2+}$ can only be characterized by polarization-dependent measurements on a single crystal sample.[30] With this technique we are able to determine the local symmetry on the point group level, rather than just obtaining a symmetry class (*e.g.* "tetragonal"). To cover all relevant point symmetries three transitions were monitored for polarization effects: the $(^5D_0 \rightarrow {}^7F_1)$-, the $(^5D_0 \rightarrow {}^7F_2)$-, and the $(^5D_0 \rightarrow {}^7F_4)$-transition. For Eu^{3+} in the D_{2d} symmetry of the Ca^{2+} site in the powellite lattice according to Aleksandrov *et al.*[11] the $(^5D_0 \rightarrow {}^7F_4)$-transition is expected to show two peaks in σ- and a single peak in π-geometry. In S_4 symmetry the inverse pattern (1σ, 2π) should be observed in the $(^5D_0 \rightarrow {}^7F_2)$-band. Fig. 6 shows the F_1-, F_2-, and F_4-transition at four angles of rotation relative to the arbitrary plane of polarization of the laser beam (α).

None of the measured bands shows any significant dependence on the polarization plane of the laser light. The $(^5D_0 \rightarrow {}^7F_1)$-band (Fig. 6a) shows a threefold splitting as had been observed in the powder samples for all values of α. Also for the $(^5D_0 \rightarrow {}^7F_2)$-band the same fourfold splitting as for the powder sample of the same composition is observed, with no dependence on α. The observed splitting pattern and polarization dependence cannot be brought into agreement with the
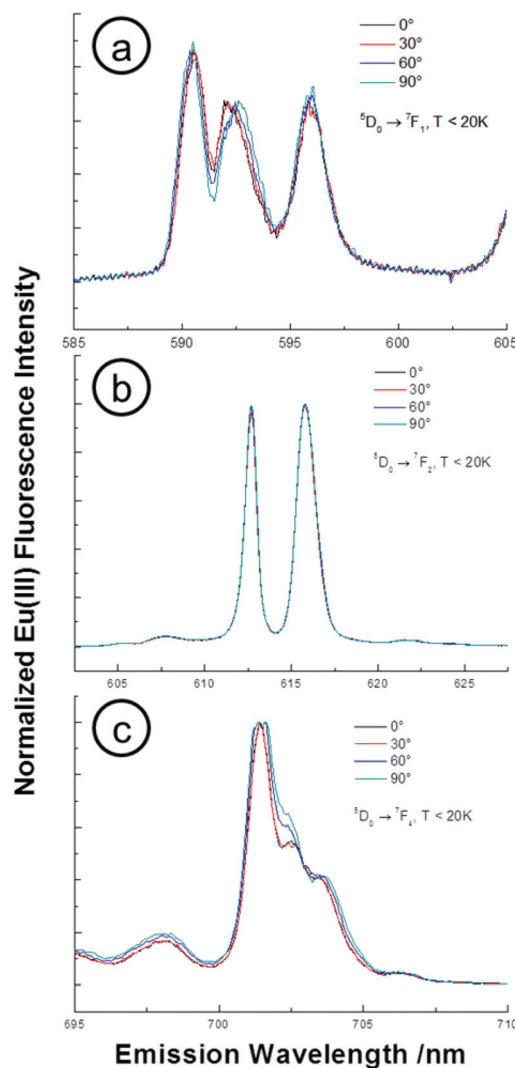

Fig. 6 Polarization-dependent measurements of the $(^5D_0 \rightarrow {}^7F_1)$-transition (a), the $(^5D_0 \rightarrow {}^7F_2)$-transition (b), and the $(^5D_0 \rightarrow {}^7F_4)$-transition (c) of NaGd(Eu)(MoO$_4$)$_2$ recorded at $T < 20$ K with the set-up described above. One out of three rotational angles α is shown for each of the bands; omitted spectra did not show additional features or changes.

expected S_4 point symmetry. The $(^5D_0 \rightarrow {}^7F_4)$-band (Fig. 6c) does not show a polarization dependence either, which also excludes the possibility of Eu^{3+} being coordinated in a D_{2d} point symmetry.

By this procedure, it becomes evident that the powellite lattice undergoes a distortion due to the substitution of Ca^{2+} by Na^+ and Gd^{3+}, as neither of the reported coordinations of the Ca^{2+} lattice site is found for the trivalent ion. Moreover, we can now fully determine the point symmetry of the local environment of Eu^{3+} and Gd^{3+}, in the end-member of the solid solution. According to the procedure laid out by Görller-Walrand and co-workers,[30] a threefold splitting in the $(^5D_0 \rightarrow {}^7F_1)$-transition with no polarization dependence and a fourfold splitting in the $(^5D_0 \rightarrow {}^7F_2)$-transition, likewise independent of polarization, is characteristic of the C_{2v} point group. Having identified the specific point symmetry of the local
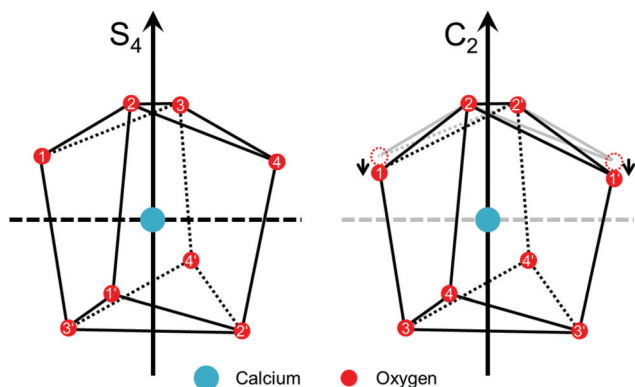
Fig. 7 Schematic representation of the Ca^{2+} lattice site in undisturbed powellite (left, reproduced from ref. 12), and in the $NaGd(MoO_4)_2$ end-member of the solid solution (right). Blue spheres represent Ca^{2+}, red spheres represent O^{2-}, large arrows represent axial symmetry elements (S_4, C_2), and small arrows show a possible mode of lattice relaxation due to the substitution. The dashed line is the mirror element of the S_4 symmetry element, which is lost upon the distortion.

coordination of the trivalent guest ion in the solid solution, it becomes possible to analyze how this coordination relates to the expected coordination in the undistorted crystal lattice.

In the structure reported by Hazen *et al.*[12] the Ca^{2+} ion is immediately surrounded by eight oxides in a S_4 point symmetry. The structure of the lattice site is schematically represented in Fig. 7 on the left. The oxides form two rectangles ([1–4] and [1′–4′], respectively), each folded along its diagonal and rotated by 90° with respect to the other rectangle. The right side of Fig. 7 shows a minor distortion that transforms the S_4 point group into the observed C_{2v} point group. The downward movement of oxygens 1 and 4 (or 1 and 1′ in the new structure) breaks the mirror element of the S_4 axis. The same applies for any concerted movement of any two oxygens that is not matched by all other oxygen atoms in the structure. If the mirror element of the S_4 symmetry element is broken, what remains is a C_2 axis, as well as two vertical mirror planes, which already exist in the S_4 point group (not shown). This is the definition of the C_{2v} point symmetry.

The observed distortion must be a consequence of the altered charge density distribution in the Ca^{2+} lattice site, due to the substitution of a di- by a mono- and a trivalent ion; it is, however, very similar to distortions that had been observed previously under the influence of high pressures.[12] We cannot determine the extent of the distortion by TRLFS, but due to the series' homogeneity, it appears reasonable to assume that it is an overall minor effect. A direct characterization of the coordination environment of the Na^+ cation in the structure is not possible with the techniques applied in this study. Based on the observation that an increased charge density in the Ca^{2+} lattice site induces a distortion it is reasonable to conclude that a decreased charge density will have a similar effect. From the fact that all members of the solid solution series exhibit identical powder diffraction patterns, one could speculate that the distortion of the Na^+ occupied Ca^{2+} lattice sites "compensates" for the distortion in the Gd^{3+} occupied sites to maintain the overall $I4_1/a$ space symmetry. The unambiguous characterization of Na^+'s coordination environment, as well as the extent of distortion in both lattice sites, will require additional research, *e.g.*, by a combination of thermodynamic and quantum mechanical calculations.

Conclusions

The investigation of the $CaMoO_4$–$NaGd(MoO_4)_2$ solid solution series by polarization-dependent site-selective TRLFS provides molecular level insight into the structural effects of the solid solution formation. The solid solution is homogeneous throughout the full composition range, with only one coordination environment for the trivalent ion. By extension this must also be the case for the monovalent ion incorporated for charge compensation. Powder X-ray diffraction confirms the homogeneity of the solid solution series, as well as the preservation of the powellite bulk crystal structure. The cations appear to be randomly distributed, and no indication of layering or other ordering phenomena has been observed.

The observation of a homogeneous composition throughout the full series range suggests an ideal solid solution behavior. This behavior will be beneficial for the immobilization of radionuclides in a waste repository scenario, as trace contaminants can be structurally incorporated even in the presence of large excess of other trivalent ions. Technical applications, *e.g.* for optical materials, should also benefit from a wide range of possible compositions, without a discernible impact on the stability.

The observed Ln^{3+} species exhibits spectroscopic characteristics of strong coordination, evidence of a strong interaction between Eu^{3+} and MoO_4^{2-}. The polarization-independence of select bands in the emission spectrum of Eu^{3+} in $NaGd(Eu)(MoO_4)_2$ reveals that the coordination environment of the trivalent ions has been distorted to C_{2v} point symmetry. This symmetry can easily be reached from the original S_4 geometry, by minor motion of the coordinating oxygen atoms, likely prompted by the higher charge density of the trivalent cation relative to Ca^{2+}.

In conclusion, powellite appears to be an ideal host for trivalent lanthanides (and actinides) due to its capability to form a solid solution over the whole composition range from trace level substitution to full cation exchange. The lattice distortion induced by the substitution is minor. It can be expected that this will positively affect the thermodynamic stability of these solid solutions. Due to the minor distortion we can assume that the loss of enthalpy due to the induced lattice distortion will be small and will be overcompensated by the gain in entropy upon formation of the mixed phase. Based on these positive results it appears worthwhile to continue studies in this system, *e.g.* with respect to the solid solution's long-term stability and thermodynamic properties.

Acknowledgements

Notes and references

1 P. Zimmer, E. Bohnert, D. Bosbach, J. I. Kim and E. Althaus, *Radiochim. Acta*, 2002, **90**, 529–535.

2 A. Abdelouas, J.-L. Crovisier, W. Lutze, B. Grambow, J.-C. Dran and R. Müller, *J. Nucl. Mater.*, 1997, **240**, 100–111.

3 D. Bosbach, T. Rabung, F. Brandt and T. Fanghänel, *Radiochim. Acta*, 2004, **92**, 639–643.

4 C. Mendoza, D. D. Ligny, G. Panczer, S. Peuget, I. Bardez-Giboire and S. Schuller, *Opt. Mater.*, 2011, **34**, 386–390.

5 R. J. Short, R. J. Hand, N. C. Hyatt and G. Möbus, *J. Nucl. Mater.*, 2005, **340**, 179–186.

6 T. Taurines and B. Boizot, *J. Am. Ceram. Soc.*, 2012, **95**, 1105–1111.

7 S. B. Stevens, C. A. Morrison, T. H. Allik, A. L. Rheingold and B. S. Haggerty, *Phys. Rev. B: Condens. Matter*, 1991, **43**, 7386–7394.

8 K. Ravindran Nair, P. Prabhakar Rao, S. Sameera, V. S. Mohan, M. R. Chandran and P. Koshy, *Mater. Lett.*, 2008, **62**, 2868–2871.

9 M. Thomas, P. Prabhakar Rao, S. P. K. Mahesh, V. R. Reshmi, T. Linda Francis and P. Koshy, *J. Am. Ceram. Soc.*, 2012, **95**, 2260–2265.

10 L. Macalik, J. Hanuza, B. Macalik, W. Strek and J. Legendziewicz, *Eur. J. Solid State Inorg. Chem.*, 1996, **33**, 397–410.

11 V. B. Aleksandrov, L. V. Gorbatyi and V. V. Ilyukhin, *Crystallogr. Rep.*, 1968, **13**, 414–415.

12 R. M. Hazen, L. W. Finger and J. W. E. Mariathasan, *J. Phys. Chem. Solids*, 1985, **46**, 253–263.

13 J. Hanuza, A. Haznar, M. Maczka, A. Pietraszko, A. Lemiec, J. H. v. d. Maas and E. T. G. Lutz, *J. Raman Spectrosc.*, 1997, **28**, 953–963.

14 U. Kolitsch, *Z. Kristallogr.*, 2001, **216**, 449–454.

15 M. Schmidt, T. Stumpf, M. M. Fernandes, C. Walther and T. Fanghänel, *Angew. Chem., Int. Ed.*, 2008, **47**, 5846–5850.

16 T. Schustereit, S. L. Müller, T. Schleid and I. Hartenbach, *Crystals*, 2011, **1**, 244–253.

17 J. Bruno, D. Bosbach, D. A. Kulik and A. Navrotsky, *Chemical Thermodynamics of Solid Solutions of Interest in Nuclear Waste Management*, OECD Publishing, London, 2007.

18 K. Holliday, A. Chagneau, M. Schmidt, F. Claret, T. Schäfer and T. Stumpf, *Dalton Trans.*, 2012, **41**, 3642–3647.

19 M. Schmidt, T. Stumpf, C. Walther, H. Geckeis and T. Fanghänel, *Dalton Trans.*, 2009, 6645–6650.

20 M. M. Fernandes, T. Stumpf, T. Rabung, D. Bosbach and T. Fanghänel, *Geochim. Cosmochim. Acta*, 2008, **72**, 464–474.

21 R. J. Reeder, M. Nugent, G. M. Lamble, C. D. Tait and D. E. Morris, *Environ. Sci. Technol.*, 2000, **34**, 623–644.

22 T. Stumpf, H. Curtius, C. Walther, K. Dardenne, K. Ufer and T. Fanghänel, *Environ. Sci. Technol.*, 2007, **41**, 3186–3191.

23 M. Schmidt, T. Stumpf, C. Walther, H. Geckeis and T. Fanghänel, *J. Colloid Interface Sci.*, 2010, **351**, 50–56.

24 K. Binnemans and C. Görller-Walrand, *J. Alloys Compd.*, 1997, **250**, 326–331.

25 W. T. Carnall, in *Handbook on the Physics and Chemistry of Rare Earths*, North Holland Publishing, Amsterdam, 1979, pp. 171–206.

26 G. R. Choppin and D. R. Peterman, *Coord. Chem. Rev.*, 1998, **174**, 283–299.

27 G. R. Choppin and Z. M. Wang, *Inorg. Chem.*, 1997, **36**, 249–252.

28 S. T. Frey, J. William De and W. Horrocks, *Inorg. Chim. Acta*, 1995, **229**, 383–390.

29 D. E. Henrie, R. L. Fellows and G. R. Choppin, *Coord. Chem. Rev.*, 1976, **18**, 199–224.

30 C. Görller-Walrand and K. Binnemans, in *Handbook on the Physics and Chemistry of Rare Earths*, ed. J. K. A. Gschneidner and L. Eyring, Elsevier Science B.V., Amsterdam, 1996, vol. 23, pp. 121–284.

31 *Lanthanide Probes in Life, Chemical and Earth Sciences*, ed. J. C. G. Bünzli and G. R. Choppin, Elsevier, Amsterdam, 1989.

32 T. Kimura, Y. Kato, H. Takeishi and G. R. Choppin, *J. Alloys Compd.*, 1998, **271–273**, 719–722.

33 W. D. Horrocks Jr. and D. R. Sudnick, *J. Am. Chem. Soc.*, 1979, **101**, 334–340.

34 W. D. Horrocks, B. Holmquist and B. L. Vallee, *Proc. Natl. Acad. Sci. U. S. A.*, 1975, **72**, 4764–4768.

35 W. D. Horrocks and D. R. Sudnick, *Acc. Chem. Res.*, 1981, **14**, 384–392.

36 C. Edder, C. Piguet, J.-C. G. Bünzli and G. Hopfgartner, *Chem.–Eur. J.*, 2001, **7**, 3014–3024.

37 T. Förster, *Ann. Phys.*, 1948, **437**, 55–75.

38 D. L. Dexter, *J. Chem. Phys.*, 1953, **21**, 836–850.

39 R. D. Shannon, *Acta Crystallogr., Sect. A: Cryst. Phys., Diffr., Theor. Gen. Cryst.*, 1976, **32**, 751–767.

40 N. Huittinen, T. Rabung, J. Lutzenkirchen, S. C. Mitchell, B. R. Bickmore, J. Lehto and H. Geckeis, *J. Colloid Interface Sci.*, 2009, **332**, 158–164.

41 V. L. Vinograd, D. Bosbach, B. Winkler and J. D. Gale, *Phys. Chem. Chem. Phys.*, 2008, **10**, 3509–3518.

42 M. Albin and W. D. Horrocks, *Inorg. Chem.*, 1985, **24**, 895–900.